

Specific and Selective Peptide-Membrane Interactions Revealed Using Quartz Crystal Microbalance

Adam Mechler,* Slavica Praporski,* Kiran Atmuri,* Martin Boland,[†] Frances Separovic,[†] and Lisandra L. Martin*

*School of Chemistry, Monash University, Clayton, Victoria 3800, Australia, and [†]School of Chemistry, Bio21 Institute, University of Melbourne, Melbourne, Victoria 3010, Australia

ABSTRACT The skin secretions of Australian tree frogs are rich in peptides with potential antimicrobial activity. They interrupt bacterial cell membranes, although precisely how and whether all peptides have the same mechanism is not known. The interactions of three of these peptides—aurein 1.2, maculatin 1.1, and caerin 1.1 with supported phospholipid bilayers—are examined here using quartz crystal microbalance and atomic force microscopy. These approaches enabled us to reveal variations in material structure and density as a function of distance from the sensor surface when comparing mass sensorgrams over a range of harmonics of the natural resonance of the sensor crystal and hence obtain for the first time to our knowledge a mechanistic assessment of membrane disruption. We found that caerin inserted into the bilayer in a transmembrane manner, regardless of concentration and phospholipid composition consistent with a pore-forming mechanism. In contrast, maculatin and aurein interacted with membranes in a concentration-dependent manner. At low concentrations (<5 μM), maculatin exhibited transmembrane incorporation whereas aurein was limited to surface association. Upon reaching a threshold value of concentration, both peptides lysed the membrane. In the case of maculatin, the lysis progressed in a slow, concentration-dependent manner, forming mixed micelles, as shown by atomic force microscopy imaging. Aurein-induced lysis proceeded to a sudden disruption, which is consistent with the “carpet” mechanism. Both maculatin and aurein exhibit specificity toward phospholipids and thus have potential as candidates as antimicrobial drugs.

INTRODUCTION

Antimicrobial defense of various living organisms relies on specialized peptides. From plants through insects to vertebrates, including humans, various classes of peptides serve the same antimicrobial purpose. A common feature of such natural antimicrobial systems is that the action mechanism prevents the development of pathogen resistance by, e.g., disrupting the outer membrane of bacterial cells. Accordingly, these peptides are frequently considered for wide spectrum antibiotic use in human (and veterinary) medicine.

A characteristic group of antimicrobial peptides is of amphibian origin. The skin secretions of Australian tree frogs are rich in antibacterial peptides (1), which exert their bioactivity by attacking the cell membrane. These peptides, which have wide-spectrum antibacterial properties, are released in the skin secretions when the frog is under stress. This process of membrane disruption was studied in particular for the peptides aurein 1.2, maculatin 1.1, and caerin 1.1 (hereafter referred to without numerical designations). The amino acid sequences (2–5) are given in Table 1.

These peptides are cationic around neutral pH with a net positive charge. Structural features include a tendency toward random coil arrangement in aqueous solution and an α -helical conformation in membrane mimetic environments (2–5). The helices are amphipathic with polar side chains aligning along one face of the α -helix. Each of the peptides is

also C-terminal aminated, and it is believed that this functional group is essential for antibacterial action (6). Concerning peptide length and conformation in membrane mimetic environments, two different geometries can be distinguished. Whereas aurein adopts a single continuous α -helix upon membrane binding, the longer peptides comprise a flexible hinge region separating two α -helices. Maculatin contains one proline residue, whereas caerin has two proline residues, which act to form a hinge region (5,7). The presence of the proline residue affects the activity of maculatin (8) and caerin (9).

Based on structural features, two principal modes of membrane-disrupting action have been proposed: transmembrane pore formation “puncturing” the lipid bilayer or a surface-associated “carpet” mechanism, lysing the membrane in a detergent-like manner (10). The transmembrane models involve the peptides forming pores through the membrane by the “barrel-stave” (11) and toroidal pore (12,13) mechanisms. Preference for barrel-stave versus toroidal pore may depend on several factors, including the peptide length and membrane-thinning effect induced by the peptide (11,14). Peptides with 20 or more amino acids are able to span the lipid bilayer when in an α -helical conformation and for the transmembrane action are predicted to be aligned perpendicular to the membrane surface at high concentrations (14). In the carpet model, peptides may lie along the membrane surface before disrupting the bilayer in a detergent-like manner once a threshold concentration is reached (15,16). It has also been suggested that this model is simply an extreme form of the toroidal pore model (17).

Submitted July 2, 2007, and accepted for publication August 8, 2007.

Address reprint requests to Lisandra L. Martin, Tel.: 613-99054514; Fax: 613-99054514; E-mail: Lisa.Martin@sci.monash.edu.au.

Editor: Peter Hinterdorfer.

TABLE 1 Amino acid sequence of selected antibacterial peptides from Australian tree frogs

Peptide	Amino acid sequence	MW	AA	Net charge
Aurein 1.2	GLFDIHKIAESF-NH ₂	1478	13	+1
Maculatin 1.1	GLFGVLAKVAAHVVPVPAIAEHF-NH ₂	2145	21	+3
Caerin 1.1	GLLSVLGSAKHVLPVVPVIAEHL-NH ₂	2582	25	+3

A range of biophysical techniques has been used to determine which of these mechanisms are implemented by individual peptides. Most of these techniques employ model membrane systems. Zwitterionic phosphatidylcholine lipids (e.g., palmitoyl-oleoyl-phosphatidylcholine, POPC) and anionic phosphatidylglycerols (e.g., palmitoyl-oleoyl-phosphatidylglycerol, POPG) are used as models for eukaryotic and bacterial membranes, respectively (18). Monolayer studies of maculatin (19) reveal that, when mixed with POPC, the peptide and lipid appear to form domains in the monolayer. However, in films with POPG, the peptides show miscible behavior, which may relate to the specific lytic activity of these peptides in bacterial membranes as opposed to red blood cells.

Solid-state NMR studies of the interaction of these peptides have been undertaken using model membranes of the zwitterionic phospholipid, dimyristoyl-phosphatidylcholine (DMPC) (20,21). Deuterated DMPC was used to ascertain the interaction of the peptides with the lipid acyl chains. Changes were seen in the NMR spectra of both the head-group (³¹P) and alkyl chain regions (²H) of the lipid molecules upon addition of the peptides to DMPC bilayers. However, the interaction with DMPC is only peripheral and the lipid bilayer phase was preserved even under high peptide concentrations. In addition, ¹⁵N-NMR of specifically labeled peptides in aligned DMPC bilayers was used in an effort to determine the orientation of the peptides within the lipid bilayer. However, for the ¹⁵N studies (20,21), cross-polarization was extremely difficult to achieve, which suggests that the peptides are highly mobile. In addition, since the ³¹P and ²H spectra were consistent with a fluid phase lipid bilayer with little effect of peptides even at high concentrations, the data indicated that the peptides do not appear to interact significantly with zwitterionic lipids. A stronger interaction with anionic phospholipids would support a preferential interaction with bacterial membranes.

³¹P-NMR spectroscopy of live Gram-positive bacteria showed that inoculation with maculatin or caerin causes a loss of integrity of the bacterial membrane resulting in an increase in isotropic signal (22). The change in the ³¹P spectra was interpreted as showing that the bacterial membranes were lysed and resulted in the formation of micelle-like structures. Although these experiments indicate that maculatin and caerin may operate via the carpet model, studies in model phospholipid membranes suggest a pore-forming mechanism (18). Electron microscopy results show that maculatin severely disintegrates cells of *Staphylococcus aureus* (5,6), which suggests that in the case of the live

bacteria, an extreme case of toroidal pores could be the cause of the isotropic ³¹P-NMR signal.

Fluorescence spectroscopy was used to assess the lytic activity of these peptides with large (LUV) and giant unilamellar vesicles (GUV) (23) formed from POPC and POPC/POPG (1:1, molar). Maculatin and mutant peptides, where Pro-15 is replaced by Gly or Ala, show similar levels of lytic activity in zwitterionic LUV. However, the lytic potency of the mutants is reduced tenfold in anionic vesicles, which suggests that proline in maculatin may play a key role in the antibacterial activity. GUV are completely destroyed by addition of the shorter sequence peptide aurein. However, in contrast to the maculatin peptides, a high peptide/lipid ratio is needed to achieve dye leakage. Addition of maculatin caused differential quenching of different sized fluorescence probes, indicating that this peptide forms pores through which the smaller probe is able to escape from the GUV. The peptide length may be the origin of the distinction because the longer peptides are able to adopt a transbilayer configuration, leading to oligomerization and formation of a pore, whereas the bilayer character is preserved. It is suggested that the shorter sequence peptides interact with the membrane but due to a mismatch between the peptide length and the bilayer thickness, the carpet mechanism leads to membrane destabilization. Nevertheless, the mode of action remains unclear.

Quartz crystal microbalance (QCM) studies on deposition of phospholipid bilayers and vesicular layers from liposome solutions suggest that an artificial membrane of controlled character can be formed in situ (24–29). QCM, when correlating mass changes measured by using different harmonics (overtones) of the sensor crystal, is able to provide information about the spatial distribution of mass change related to the sensor surface (30–32). Consistently, this method can be used to investigate the mass and structural changes caused by the insertion of peptides and/or the removal of lipid thereby. Although a few feasibility studies have been published (33,34), no detailed works have used QCM to study structural aspects of membrane disruption thus far.

Atomic force microscopy (AFM) imaging of surface-confined membranes and membrane-protein systems has been published by several authors (35–42). Membrane disruption by antimicrobial peptides, however, was primarily studied on whole bacterial cells and only a few works have used model membranes (43–45), which is necessary to achieve high resolution. Furthermore, although dynamic processes such as lipid membrane formation and phase

transitions have been imaged before (46,47), in the case of membrane-disrupting peptides, AFM studies are limited to before-after pictures and do not attempt to follow the process in real time.

Here we report results using the short peptide aurein and the longer membrane-spanning peptides that exhibit pronounced kinks associated with the proline residues maculatin and caerin. Features exhibited by both pore-forming and membrane-disruptive (carpet-like) mechanisms were elucidated by correlating QCM and AFM measurements.

MATERIALS AND METHODS

Liposome preparation

1,2-Dimyristoyl-*sn*-glycero-3-phosphocholine (DMPC) and 1,2-dimyristoyl-*sn*-glycero-3-phospho-*rac*-(1-glycerol) (DMPG) were purchased from Avanti Polar Lipids (Alabaster, AL). Chloroform and methanol were purchased from Sigma-Aldrich (St. Louis, MO).

Chip cleaning and surface modification

Ethanol absolute, acetone, propan-2-ol, and hydrogen peroxide (30%) were purchased from Merck (Melbourne, Australia). Ammonia solution (28%) was purchased from Ajax Finechem (Sydney, Australia). 3-Mercaptopropionic acid (MPA) was purchased from Fluka, BioChimica (Buchs, Switzerland).

Buffers

Sodium chloride, potassium phosphate monobasic, and potassium phosphate dibasic were purchased from Sigma-Aldrich. Ultrapure water with a resistivity of 18.2 M Ω was used (Sartorius, Goettingen, Germany).

Peptides

Aurein 1.2, caerin 1.1, and maculatin 1.1 were custom-made by Mimotopes (Melbourne, Australia) by solid-phase synthesis and assessed by mass spectrometry and high performance liquid chromatography with purity >90%.

Liposome preparation protocol

DMPC was dissolved in chloroform and DMPG in CHCl₃/methanol (75:25 v/v) to create individual stock solutions. These stock solutions were then dispensed out into test tubes in the desired ratios of DMPC or DMPC/DMPG (4:1) and the solvent was evaporated under a gentle stream of N₂ and dried under vacuum for 40 min. Liposomes were prepared as previously described (42,48); in brief, lipids were resuspended in 20 mM phosphate buffered saline (100 mM NaCl at pH 6.8), vortexed, and briefly sonicated before use.

Quartz crystal microbalance with dissipation monitoring

QCM with dissipation monitoring (QCM-D) measurements were performed with the Q-SENSE E4 system (Q-SENSE, Västra Frölunda, Sweden). The sensor crystals used were 5 MHz, AT-cut, polished quartz discs (chips) with evaporated gold sensor surface. The mass sensitivity in aqueous measurements was \sim 1.8 ng/cm² in E4.

The change of resonance frequency (Δf) and energy dissipation (ΔD) upon mass deposition were measured simultaneously at four different

overtones of the natural frequency (third overtone at 15 MHz, fifth overtone at 25 MHz, seventh overtone at 35 MHz, and ninth overtone at 45 MHz) as well as at natural frequency. The Δf and ΔD values of the seventh overtone (35 MHz) were presented, if not stated otherwise. Measurements at natural frequency (5 MHz) were not considered due to this resonance being very sensitive to bulk solution changes and generating unreliable data. The working temperature was 19°C. A flow-through system allowed successive application of a set of sample fluids to the sensor. Before assembling into the chamber, sensor chips were rinsed with ethanol and dried under a gentle stream of N₂ gas, after which they were placed into a 1:1:3 solution of ammonia, hydrogen peroxide, and water at \sim 75°C for 15–20 min. Subsequently, chips were thoroughly rinsed with ultrapure water and ethanol, dried, and immediately assembled into the QCM-D chamber ready to use. One chip was used to perform at least 10 experiments.

The gold surface of the chip was chemically modified *in situ* before liposome deposition. A clean gold crystal was treated with MPA to form a self-assembled monolayer of uniform negatively charged surface as a support for the artificial membrane (48). This process was typically 20 min in duration, using a 1 mM solution of MPA in propan-2-ol.

A typical experiment involved two main stages after MPA modification of the gold crystal (Fig. 1): lipid deposition, which required about 1 h for a stable lipid bilayer to form, and introduction of the peptide and subsequent monitoring of the membrane-disrupting action. The original data were analyzed by graphing software Origin 7.5 (OriginLab, Northampton, MA).

QCM experiments were repeated 3–5 times for each peptide and at each concentration. Small frequency variations were observed; however, these correlated with the amount of lipid. For the same lipid mass, the peptide response was reproducible within 1 Hz, that is, within the sensitivity of the instrument.

Atomic force microscopy

AFM imaging was performed with an Ntegra Scanning Probe Laboratory (NT-MDT, Moscow, Russia) by using intermittent contact (“tapping”) mode in physiological buffer solution (20 mM phosphate buffer with 100 mM NaCl at pH 6.8). NSC36B probes (MikroMasch, Tallinn, Estonia) were used. Consecutive 512 \times 512 pixel images were captured with an \sim 8 min frame rate.

A total of 0.5 μ M DMPC was deposited to freshly cleaved mica surface, incubated for 5 min at 37 C, and then rinsed with droplets of buffer. Imaging was performed on regions of exposed membrane boundaries, where the underlying mica surface can be clearly distinguished. After images of the

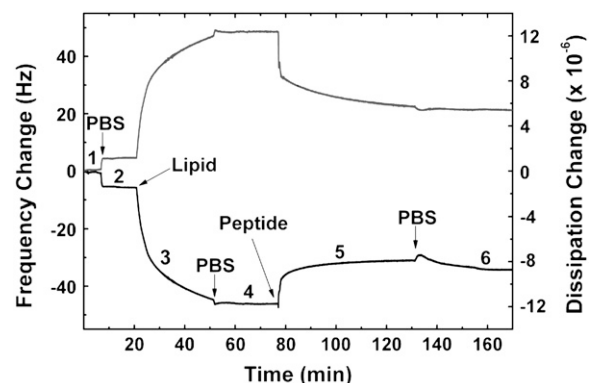


FIGURE 1 Typical sensorgram of a QCM experiment (DMPC, 10 μ M maculatin). (1) Initial water baseline; (2, 4, and 6) buffer baselines; (3) lipid deposition curve, and (5) peptide effect. A difference in frequency between baselines 2 and 4 was used to calculate a total amount of lipid on the chip surface. The positive change in frequency between baselines 4 and 6 suggests a mass loss due to the peptide action on a phospholipid bilayer.

membrane have been obtained and the static nature of the membrane confirmed, peptide solution was injected without stopping imaging to maintain the timeline. The effect of peptide exposure was thus observed in real time. AFM images reveal specific morphology, which is distinguishable and recognizable for each peptide-membrane interaction. Imaging was repeated twice for each peptide.

RESULTS AND DISCUSSION

The interaction between aurein, maculatin, and caerin with supported phospholipid bilayers composed of either DMPC or DMPC/DMPG (4:1) was assessed using QCM. In each case, phospholipid surfaces were prepared *in situ* and a stable baseline was obtained before exposure to the peptide and analysis of the effects. Data were recorded as frequency change where decrease corresponds to an increase in mass on the modified chip (49). In each case, the dissipation parameter (data not shown) reflected the structural changes indicated by the frequency response, thus confirming our analysis and conclusions.

Concentration dependence of DMPC membrane disruption

First, the effect of the three peptides on DMPC bilayers was assessed. Typical QCM traces are shown in Fig. 2. Upon introduction into the measurement cell, the peptides interacted with the membrane immediately. Initial decrease in QCM frequency suggests mass uptake for all three peptides. For caerin, the mass uptake continued for all concentrations, proceeding to saturation. Since the final mass

uptake was proportional to the concentration, this could be interpreted as depletion of peptides and the achievement of a steady state in the reacting volume. Saturation of the membrane occurred at higher peptide concentrations.

Maculatin proceeded with proportional mass uptake up to $5 \mu\text{M}$ concentration, and then the shape of the curve revealed a change in mechanism: after reaching a threshold concentration within the membrane, a slow mass removal began (Fig. 2 *e*). At higher concentrations the mass removal became dominant.

For aurein, the trace was somewhat different to the other two peptides: saturation was reached sooner, assessed by a flat line, suggesting a dynamic equilibrium between membrane-bound and solution phase species. As concentration was increased, the initial mass gain moved toward net mass removal, similar to that observed for maculatin.

Analysis of frequency changes at different harmonics

Recording mass change using different overtones of the natural frequency of the QCM sensor chip provides a means of characterizing processes as a function of distance from the surface (30–32). Although a discrete sectioning cannot be achieved, transmembrane and surface effects can be simply distinguished. In Fig. 3, a representative set of third, fifth, seventh, and ninth overtone QCM traces of the exposure of DMPC membrane to $7 \mu\text{M}$ peptide solutions is shown. The first overtone was not used, as it senses mostly the solution and thus gives meaningless information. For caerin, the mass

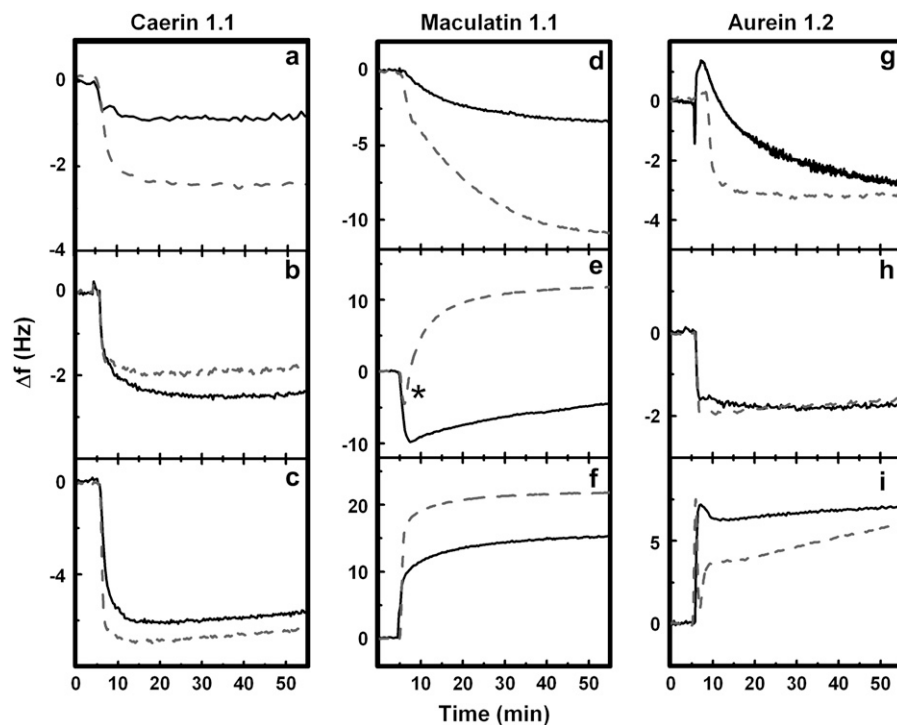


FIGURE 2 Typical QCM traces of the effect of the three peptides at different concentrations on DMPC bilayers. (Solid trace in *a*, *d*, and *g*: $1 \mu\text{M}$; *b*, *e*, and *h*: $5 \mu\text{M}$; and *c*, *f*, and *i*: $10 \mu\text{M}$ peptide concentration; dashed trace in *a*, *d*, and *g*: $2 \mu\text{M}$; *b*, *e*, and *h*: $7 \mu\text{M}$; and *c*, *f*, and *i*: $20 \mu\text{M}$ peptide concentration.)

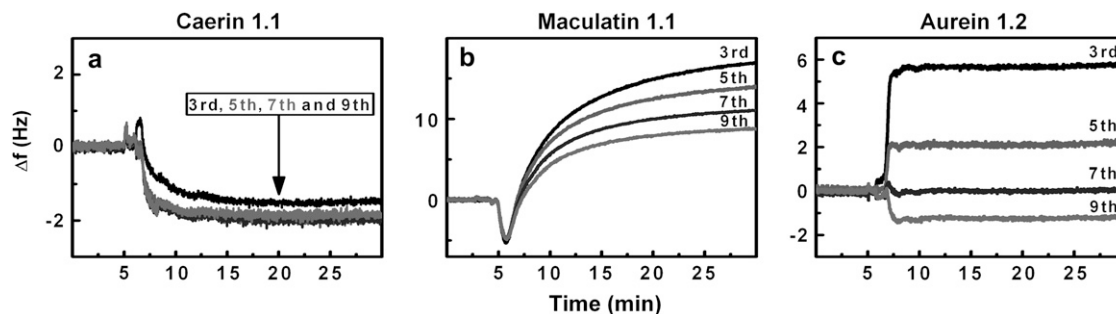


FIGURE 3 Overtone effect for the three peptides at $7 \mu\text{M}$ on DMPC. (a) Caerin: there is no significant difference between the traces, suggesting transmembrane insertion; (b) maculatin: there are slight differences in the disruption phase, and (c) aurein, the difference between the overtones reveals a surface process.

measured by all overtones was the same, indicating a process that has the same structural characteristics across the whole thickness of the membrane, consistent with a vertical transmembrane insertion. Maculatin initially behaved in a similar manner. However, once the insertion process changed to membrane removal, different masses were recorded. This suggests an initial transmembrane insertion, followed by an asymmetrical disruption mechanism once a threshold concentration was reached. Aurein, on the other hand, behaved differently: lower overtones indicated mass removal whereas higher overtones, those that probe processes closer to the sensor surface, showed mass increase. This behavior can be explained by a structural effect: surface association of the peptide changes the interface between the membrane and the water, which affects the coupling of the oscillation energy into the aqueous media. Thus, even without actual material removal, the third overtone would indicate mass loss as the movement of the surface would drag a lower amount of water. The ninth overtone, which is dissipated mostly within the membrane, senses the additional mass of the peptide on the bilayer.

A summary of the overtone effects as a function of concentration is depicted as a bar chart in Fig. 4. For caerin, identical mass changes at all four overtones indicate that transmembrane insertion was dominant, although at higher concentrations some surface adsorption might also have occurred. Importantly, membrane removal did not occur even at high peptide concentrations. Transmembrane insertion dominated at lower concentrations of maculatin, with slow material removal seen at $5 \mu\text{M}$. From $7 \mu\text{M}$ and higher concentrations, disruption was the primary process. A different mechanism was observed for aurein. Concentration-independent surface association dominated the low range, with apparent material removal at lower, and mass gain at higher, overtones. Net material removal occurred from $10 \mu\text{M}$ and higher concentrations. Based on these results, aurein appeared to act on the surface of the membrane bilayer.

In context of the literature models of membrane disruption, we propose that caerin acts as a pore-forming peptide by inserting across the membrane. Aurein appeared to adopt

the mechanism known as carpet, where sudden disruption occurs after a certain threshold is reached. Maculatin, however, seemed to switch from transmembrane insertion to lysis above a threshold concentration.

Concentration and harmonic effects of DMPC/DMPG (4:1) membrane disruption

The study was extended to include the effect of membrane composition by the addition of 20% DMPG in the bilayer.

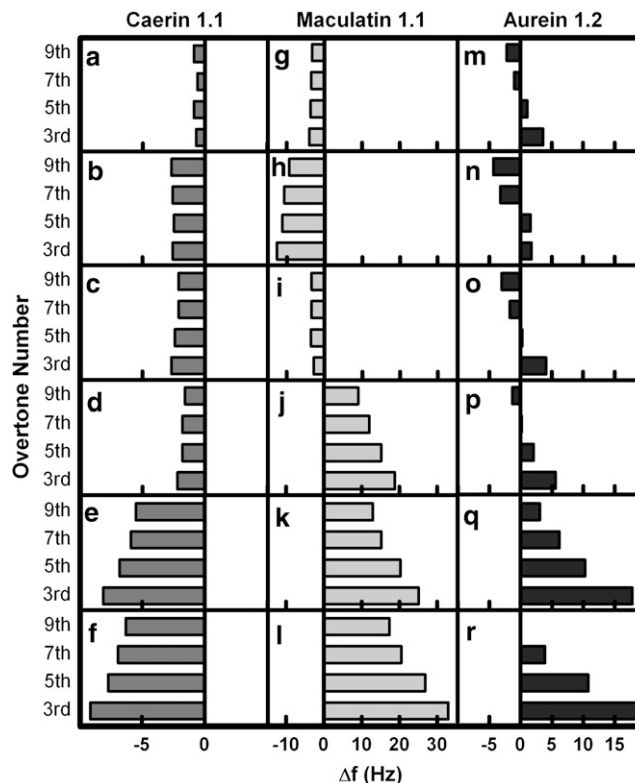


FIGURE 4 Overtone effects showing change in frequency (Hz) as a function of peptide concentration for DMPC bilayers. (a, g, and m represent $1 \mu\text{M}$; b, h, and n: $2 \mu\text{M}$; c, i, and o: $5 \mu\text{M}$; d, j, and p: $7 \mu\text{M}$; e, k, and q: $10 \mu\text{M}$; and f, l, and k: $20 \mu\text{M}$ of the peptide.)

Typical QCM traces are shown in Fig. 5. When comparing overtone effects (Fig. 6) with caerin in mixed bilayers to those in pure DMPC bilayers, no significant changes are visible, with the exception of a slow mass removal apparent at 20 μM concentration (Fig. 6 *f*). This behavior suggests that when a threshold concentration within the membrane is reached, caerin is also able to form mixed micelles and thus incite material removal. This did not lead, however, to complete material removal at higher concentrations (data not shown), confirming that the primary action remains by pore formation.

Maculatin exhibited a different behavior: from 5 μM concentration, there was surface adsorption in addition to trans-membrane insertion and a slow, partial material removal at 10 μM (Fig. 6 *k*). Importantly, large-scale membrane disruption, as observed for DMPC, did not occur. In contrast, aurein had a lower threshold with material removal at 2 μM concentration in mixed lipid layers. Specifically, the association phase at 1 μM had a different mechanism (Fig. 6 *m*), suggesting membrane incorporation as opposed to the surface association observed for DMPC alone. The conclusion is that both aurein and maculatin are lipid-selective peptides.

AFM imaging of disruption mechanism

The dynamics of membrane activity (insertion and disruption) for caerin and maculatin were further examined using AFM imaging. As a three-dimensional imaging tool, AFM is able to visualize the morphological changes of the membrane

and thus identify the differences in mechanism revealed by the QCM measurements. Imaging was performed on DMPC membranes at the phase transition temperature, where both fluid and crystalline phases are present. The membrane appeared a featureless smooth surface, with domains of crystalline and fluid phase exhibiting different heights (e.g., Fig. 7, frames 1 and 2).

In situ addition of caerin did not result in a visible change of the membrane structure, even when the concentration was increased to 100 μM (data not shown). High-resolution imaging on the membrane surface was unable to find any pore structures. This is not unexpected due to the high mobility of the peptides (and thus the pores) within the membrane. This interpretation is consistent with data obtained with solid-state NMR (20,21). The absence of peptides on the surface, and the lack of any visible disruption, is consistent with the proposed vertical insertion of peptides with a high likelihood of pore formation although the presence of pores could not be proven directly.

In contrast, the data obtained by addition of maculatin resulted in visible changes. A sequence of consecutive images of the membrane disruption is shown in Fig. 7. Images were recorded on $5 \times 5 \mu\text{m}$ areas, here the $1.2 \times 1.2 \mu\text{m}$ offline zoom sequences are shown. A movie of the full-scale sequence is available as Supplementary Material. The resolution was deliberately set low, so that the large-scale disruption events could be better observed. The first two frames show the membrane before peptide injection. The domains are static; no changes can be observed. Injection of

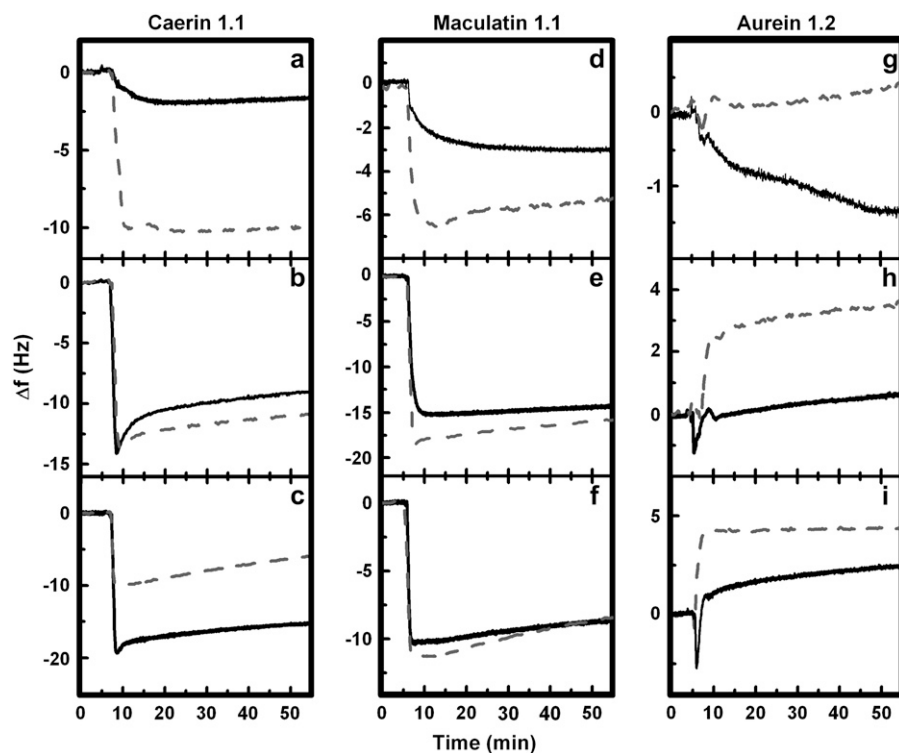


FIGURE 5 Typical QCM traces of the effect of the three peptides at different concentrations on DMPC/DMPG (4:1) bilayers. (Solid trace in *a*, *d*, and *g*: 1 μM ; *b*, *e*, and *h*: 5 μM ; and *c*, *f*, and *i*: 10 μM peptide concentration; dashed trace in *a*, *d*, and *g*: 2 μM ; *b*, *e*, and *h*: 7 μM ; and *c*, *f*, and *i*: 20 μM peptide concentration.)

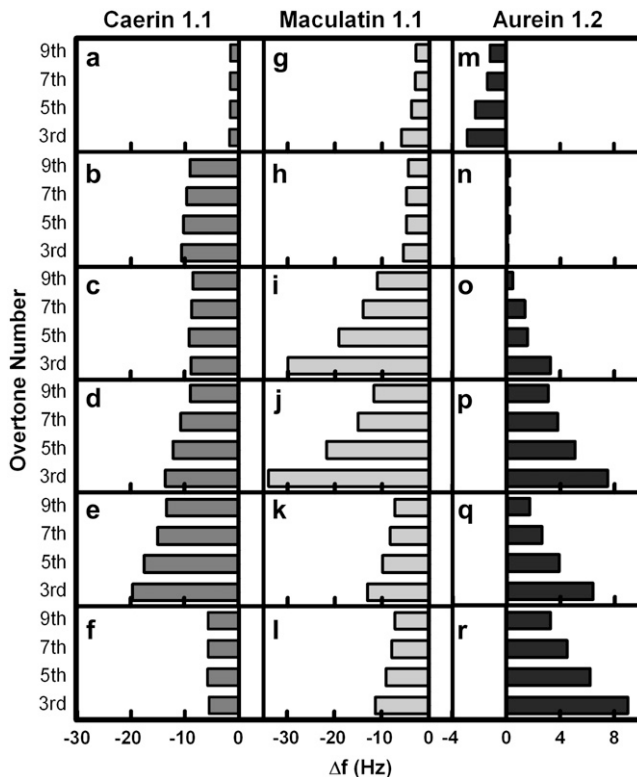


FIGURE 6 Overtone effects showing change in frequency (Hz) as a function of peptide concentration for DMPC/DMPG (4:1) bilayers. (*a*, *g*, and *m* represent $1 \mu\text{M}$; *b*, *h*, and *n*: $2 \mu\text{M}$; *c*, *i*, and *o*: $5 \mu\text{M}$; *d*, *j*, and *p*: $7 \mu\text{M}$; *e*, *k*, and *q*: $10 \mu\text{M}$; and *f*, *l*, and *r*: $20 \mu\text{M}$ of the peptide.)

peptide to a $\sim 5 \mu\text{M}$ concentration at frame 3 did not result in disruption, although some swelling of the taller (crystalline) domain can be observed, which may be the result of peptide incorporation or phase transition. A second injection of peptides to $\sim 15 \mu\text{M}$ occurred at frame 6. Visible membrane disruption is apparent and starts at frame 8 and the lower, fluid phase domain is fully disrupted by the consecutive frame. A further injection of peptide to $\sim 35 \mu\text{M}$ concentration at frame 10 resulted in a gradual disruption of the crystalline membrane domains, starting from the edges and proceeding inward. Small round objects incorporated in the membrane, possibly unopened small liposomes, appeared to

slow down disruption and play a major role in keeping some “islands” intact after most of the membrane has been removed from the surface. After disruption, a layer of $\sim 1 \text{ nm}$ high fragments, most likely peptide-lipid complexes, remain on the surface. This layer propagates from the membrane covered area across the surface. Importantly, at this resolution (pixel size $\sim 5.8 \text{ nm}$) individual peptides cannot be distinguished.

The time evolution of the three-dimensional morphology by AFM, together with the QCM data, provides a basis for speculation for the mechanism of antimicrobial peptide action. The QCM results indicate maculatin incorporation into the bilayer in a transmembrane manner at lower solution phase concentrations. However, upon reaching a threshold concentration within the membrane, disruption begins. The fact that the threshold concentration has to be reached within the membrane is deduced from the curves that show significant disruption over time but indicate peptide incorporation at the beginning (Fig. 2 *e*, *). This is consistent with the AFM observations, where no significant membrane disruption was observed before increasing the concentration beyond the threshold value. We anticipate the threshold concentration required for disruption to be a function of temperature, and since the QCM and AFM operate over different temperature ranges and the concentrations in the AFM liquid cell are estimates due to the uncontrollable evaporation of the liquid, it is not feasible to directly—or quantitatively—compare these threshold values. AFM revealed, in accordance with QCM results, that lysis is not instantaneous and proceeds from the edges of the membrane inward. This suggests that the mechanism proceeds from pore formation to a weak detergent effect, without an immediate loss of the entire membrane integrity. The thin layer of debris remaining on the surface is indicative of mixed micelle formation. One can hypothesize that inhomogeneities or phase boundaries within the membrane might serve as points of micelle detachment, whereas in the bulk of the membrane the lateral pressure prohibits such processes to happen. This preference can be explained in terms of the variations in surface tension at such sites. As composition does also have a strong effect on surface tension, this may underlie the observed lipid specificity.

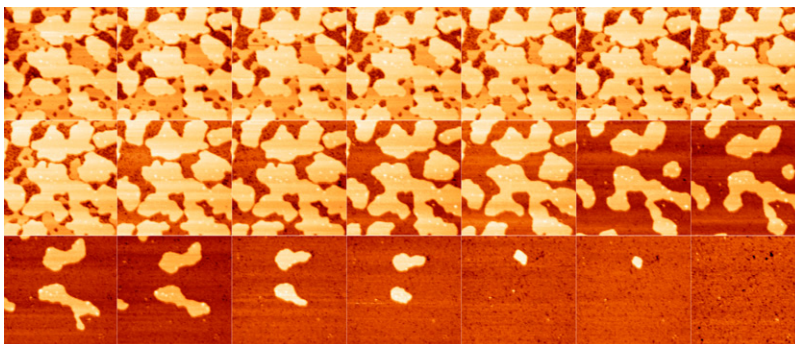


FIGURE 7 Consecutive AFM images of the membrane-disrupting effect of maculatin on DMPC bilayers. Each frame was collected in $\sim 8 \text{ min}$. The height difference between the mica substrate (*dark*) and the taller (crystalline) membrane domain was $\sim 5 \text{ nm}$. Peptide was added as follows: $\sim 5 \mu\text{M}$ concentration at frame 3; $\sim 15 \mu\text{M}$ at frame 6; and $\sim 35 \mu\text{M}$ at frame 10.

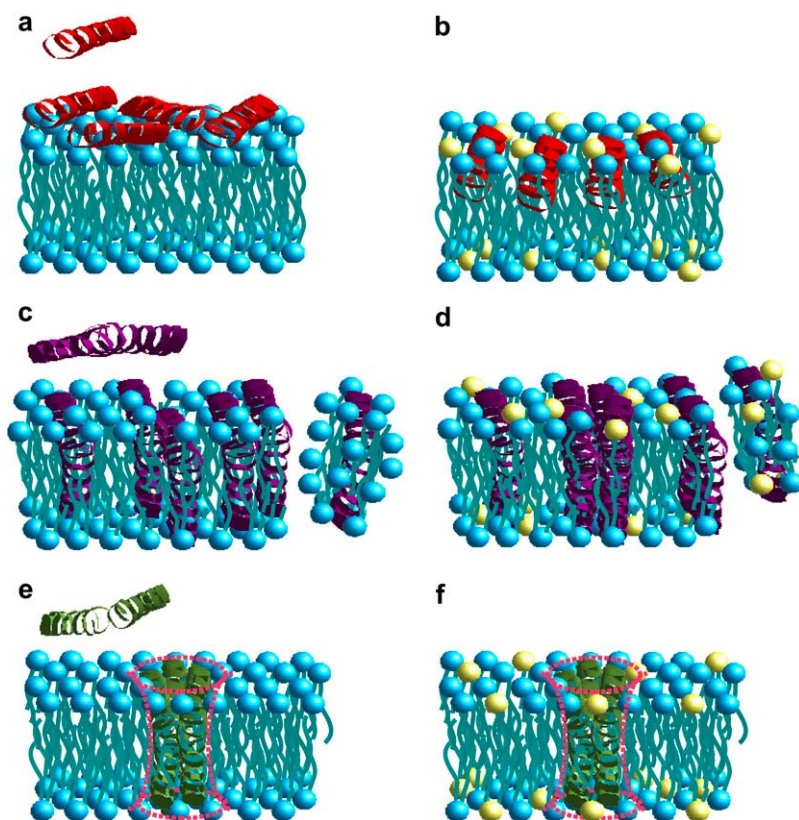


FIGURE 8 Representation for the interactions of aurein (*a* and *b*), maculatin (*c* and *d*), and caerin (*e* and *f*) peptides with supported phospholipid membranes: DMPC (*left*) and DMPC/DMPG 4:1 (*right*). Mechanisms are (*a*) surface association (carpet mechanism), (*b*) partial insertion (“detergent” mechanism), (*c* and *d*) transmembrane insertion and mixed micelle formation, and (*e* and *f*) transmembrane insertion with pore formation.

In summary, the observed peptide activities are i) aurein associates to the surface of neat DMPC (Fig. 8 *a*), initiating lysis above a threshold concentration, consistent with carpet mechanism. In contrast, in the lipid mixture, aurein interacts via partial insertion (Fig. 8 *b*), resulting in a lower lysis threshold. ii) Maculatin acts via transmembrane insertion for both lipids examined here, proceeding to full membrane lysis via mixed micelle formation for neat DMPC (Fig. 8 *c*) while remaining in the membrane (with possible small-scale mixed micelle formation at edges and domain boundaries) in the lipid mixture (Fig. 8 *d*). This implies that in the lipid mixtures, maculatin may form pores. iii) Caerin forms transmembrane pores in both DMPC and the mixture lipids (Fig. 8, *e* and *f*).

CONCLUSIONS

Here we demonstrated the membrane interactions for three amphibian antimicrobial peptides, caerin, maculatin, and aurein, with supported bilayers (DMPC and DMPC/DMPG (4:1)). We found that caerin, the longest of the three peptides, incorporated into phospholipid bilayers in a transmembrane manner, a mechanism that was qualitatively independent of concentration and lipid composition. Maculatin, however, switched from transmembrane incorporation to membrane lysis in a concentration-dependent manner while also exhibiting specificity toward phospholipids. We suggest that the

basis of such selectivity is the variation in surface tension and also the peptide sequence/length, as maculatin is just long enough to span the bilayer. Aurein associated with the upper leaflet of the membrane and acted in a carpet-like manner, also showing threshold behavior. Notably, the threshold concentration changed for different phospholipid compositions. In light of these observations, we suggest that specificity-enhanced mutants of maculatin and aurein could serve as future drug candidates and offer enormous potential for new antibiotics.

SUPPLEMENTARY MATERIAL

To view all of the supplemental files associated with this article, visit www.biophysj.org.

We are grateful for helpful discussions with Mr. Paul Barrett, ATA Scientific Ltd.

L.L.M., A.M., and F.S. gratefully acknowledge the Australian Research Council for equipment and project grants and A.M. acknowledges the award of a Monash Fellowship.

REFERENCES

1. Apponyi, M. A. A. Margit, T. L. Pukala, C. S. Brinkworth, V. M. Maselli, J. H. Bowie, M. J. Tyler, G. W. Booker, J. C. Wallace, J. A. Carver, F. Separovic, J. Doyle, and L. E. Llewellyn. 2004.

- Host-defence peptides of Australian anurans: structure, mechanism of action and evolutionary significance. *Peptides*. 25:1035–1054.
2. Rozek, T., K. L. Wegener, J. H. Bowie, I. N. Oliver, J. A. Carver, J. C. Wallace, and M. J. Tyler. 2000. The antibiotic and anticancer active aurein peptides from the Australian bell frogs *Litoria aurea* and *Litoria raniformis*. The solution structure of aurein 1.2. *Eur. J. Biochem.* 267:5330–5341.
 3. Wegener, K. L., C. S. Brinkworth, J. H. Bowie, J. C. Wallace, and M. J. Tyler. 2001. Bioactive dahlein peptides from the skin secretions from the Australian aquatic frog *Litoria dahlii*: sequence determination by electrospray mass spectrometry. *Rapid Commun. Mass Spectrom.* 15:1726–1734.
 4. Wegener, K. L., P. A. Wabnitz, J. A. Carver, J. H. Bowie, B. C. S. Chia, J. C. Wallace, and M. J. Tyler. 1999. Host defence peptides from the skin glands of the Australian Blue Mountains tree-frog *Litoria citropa*. Solution structure of the antibacterial peptide citropin 1.1. *Eur. J. Biochem.* 265:627–637.
 5. Chia, B. C. S., J. A. Carver, T. D. Mulhern, and J. H. Bowie. 2000. Maculatin 1.1, an anti-microbial peptide from the Australian tree frog, *Litoria genimaculata*. Solution structure and biological activity. *Eur. J. Biochem.* 267:1894–1908.
 6. Rozek, T., J. W. Russell, S. T. Steinborner, J. H. Bowie, M. J. Tyler, and J. C. Wallace. 1998. The maculatin peptides from the skin glands of the tree frog *Litoria genimaculata*: a comparison of the structures and antibacterial activities of maculatin 1.1 and caerin 1.1. *J. Pept. Sci.* 4:111–115.
 7. Wong, H., J. H. Bowie, and J. A. Carver. 1997. The solution structure and activity of caerin 1.1, an antimicrobial peptide from the Australian green tree frog, *Litoria splendida*. *Eur. J. Biochem.* 247:545–557.
 8. Niidome, T., K. Kobayashi, H. Arakawa, T. Hatakeyama, and H. Aoyagi. 2004. Structure activity relationship of an antibacterial peptide, maculatin 1.1, from the skin glands of the tree frog, *Litoria genimaculata*. *J. Pept. Sci.* 10:414–422.
 9. Pukala, R. L., C. S. Brinkworth, J. A. Carver, and J. H. Bowie. 2004. Investigating the importance of the flexible hinge in caerin 1.1: solution structures and activity of two synthetically modified caerin peptides. *Biochemistry*. 43:937–944.
 10. Shai, Y. 2002. Mode of action of membrane active antimicrobial peptides. *Biopolymers*. 66:236–248.
 11. Yang, L., T. A. Harroun, T. M. Weiss, L. Ding, and H. W. Huang. 2001. Barrel-stave model or toroidal model? A case study on melittin pores. *Biophys. J.* 81:1475–1485.
 12. Ehrenstein, G., and H. Lecar. 1977. Electrically gated ionic channels in lipid bilayers. *Q. Rev. Biophys.* 10:1–34.
 13. Matsuzaki, K., O. Murase, N. Fujii, and K. Miyajima. 1996. An antimicrobial peptide, magainin 2, induced rapid flip-flop of phospholipids coupled with pore formation and peptide translocation. *Biochemistry*. 35:11361–11368.
 14. Lee, M. T., F. Y. Chen, and H. W. Huang. 2004. Energetics of pore formation induced by membrane active peptides. *Biochemistry*. 43:3590–3599.
 15. Shai, Y. 1999. Mechanism of the binding, insertion and destabilization of phospholipid bilayer membranes by α -helical antimicrobial and cell non-selective membrane-lytic peptides. *Biochim. Biophys. Acta.* 1462:55–70.
 16. Shai, Y., and Z. Oren. 2001. From “carpet” mechanism to de-novo designed diastereomeric cell-selective antimicrobial peptides. *Peptides*. 22:1629–1641.
 17. Dathe, M., and T. Wiprecht. 1999. Structural features of helical antimicrobial peptides: their potential to modulate activity on model membranes and biological cells. *Biochim. Biophys. Acta.* 1462:71–87.
 18. Chia, B. C. S., J. Torres, M. A. Cooper, I. T. Arkin, and J. H. Bowie. 2002. The orientation of the antibiotic peptide maculatin 1.1 in DMPG and DMPC lipid bilayers. Support for a pore-forming mechanism. *FEBS Lett.* 512:47–51.
 19. Ambroggio, E. E., F. Separovic, J. H. Bowie, and G. D. Fidelio. 2004. Surface behaviour and peptide-lipid interactions of the antibiotic peptides, maculatin and citropin. *Biochim. Biophys. Acta.* 1664:31–37.
 20. Balla, M. S., J. H. Bowie, and F. Separovic. 2004. Solid-state NMR study of antimicrobial peptides from Australian frogs in phospholipid membranes. *Eur. Biophys. J.* 33:109–116.
 21. Marcotte, I., K. L. Wegener, Y.-H. Lam, B. C. S. Chia, M. R. R. de Planque, J. H. Bowie, M. Auger, and F. Separovic. 2003. Interaction of antimicrobial peptides from Australian amphibians with lipid membranes. *Chem. Phys. Lipids.* 122:107–120.
 22. Chia, B. C. S., Y.-H. Lam, M. Dyal-Smith, F. Separovic, and J. H. Bowie. 2000. A P-31 NMR study of the interaction of amphibian antimicrobial peptides with the membranes of live bacteria. *Lett. Pept. Sci.* 7:151–156.
 23. Ambroggio, E. E., F. Separovic, J. H. Bowie, G. D. Fidelio, and L. A. Bagatolli. 2005. Direct visualization of membrane leakage induced by the antibiotic peptides: maculatin, citropin, and aurein. *Biophys. J.* 89:1874–1881.
 24. Brian, A. A., and H. M. McConnell. 1984. Allogeneic stimulation of cytotoxic T cells by supported planar membranes. *Proc. Natl. Acad. Sci. USA.* 81:6159–6164.
 25. Keller, C. A., and B. Kasemo. 1998. Surface specific kinetics of lipid vesicle adsorption measured with a quartz crystal microbalance. *Biophys. J.* 75:1397–1402.
 26. Keller, C. A., K. Glasmästar, V. P. Zhdanov, and B. Kasemo. 2000. Formation of supported membranes from vesicles. *Phys. Rev. Lett.* 84:5443–5446.
 27. Boxer, S. G. 2000. Molecular transport and organization in supported lipid membranes. *Curr. Opin. Chem. Biol.* 4:704–709.
 28. Richter, R., A. Mukhopadhyay, and A. Brisson. 2003. Pathways of lipid vesicle deposition on solid surfaces: a combined QCM-D and AFM study. *Biophys. J.* 85:3035–3047.
 29. Richter, R. P., R. Berat, and A. R. Brisson. 2006. Formation of solid-supported lipid bilayers: an integrated view. *Langmuir*. 22:3497–3505.
 30. Wolff, O., E. Seydel, and D. Johannsmann. 1997. Viscoelastic properties of thin films studied with quartz crystal resonators. *Faraday Discuss.* 107:91–104.
 31. Hook, F., B. Kasemo, T. Nylander, C. Fant, K. Sott, and H. Elwing. 2001. Variations in coupled water, viscoelastic properties, and film thickness of a Mefp-1 protein film during adsorption and cross-linking: a quartz crystal microbalance with dissipation monitoring, ellipsometry, and surface plasmon resonance study. *Anal. Chem.* 73:5796–5804.
 32. Du, B. Y., and D. Johannsmann. 2004. Operation of the quartz crystal microbalance in liquids: derivation of the elastic compliance of a film from the ratio of bandwidth shift and frequency shift. *Langmuir*. 20:2809–2812.
 33. Steinem, C., A. Janshoff, and H. J. Galla. 1998. Evidence for multilayer formation of melittin on solid-supported phospholipid membranes by shear-wave resonator measurements. *Chem. Phys. Lipids.* 95:95–104.
 34. Snabe, T., and S. B. Petersen. 2003. Lag phase and hydrolysis mechanisms of triacylglycerol film lipolysis. *Chem. Phys. Lipids.* 125:69–82.
 35. Hansma, H. G., A. L. Weisenhorn, A. B. Edmundson, H. E. Gaub, and P. K. Hansma. 1991. Atomic force microscopy—seeing molecules of lipid and immunoglobulin. *Clin. Chem.* 37:1497–1501.
 36. Singh, S., and D. J. Keller. 1991. Atomic force microscopy of supported planar membrane bilayers. *Biophys. J.* 60:1401–1410.
 37. Schabert, F. A., C. Henn, and A. Engel. 1995. Native *Escherichia coli* OMPF porin surfaces probed by atomic force microscopy. *Science*. 268:92–94.
 38. Fang, Y., and J. Yang. 1997. The growth of bilayer defects and the induction of interdigitated domains in the lipid-loss process of supported phospholipid bilayers. *Biochim. Biophys. Acta.* 1324:309–319.
 39. Egawa, H., and K. Furusawa. 1999. Liposome adhesion on mica surface studied by atomic force microscopy. *Langmuir*. 15:1660–1666.

40. Lin, H., D. O. Clegg, and R. Lal. 1999. Imaging real-time proteolysis of single collagen I molecules with an atomic force microscope. *Biochemistry*. 38:9956–9963.
41. Reviakine, I., and A. Brisson. 2000. Formation of supported phospholipid bilayers from unilamellar vesicles investigated by atomic force microscopy. *Langmuir*. 16:1806–1815.
42. Thimm, J., A. Mechler, H. Lin, S. Rhee, and R. Lal. 2005. Calcium-dependent open/closed conformations and interfacial energy maps of reconstituted hemichannels. *J. Biol. Chem.* 280:10646–10654.
43. Rinia, H. A., J. W. P. Boots, D. T. S. Rijkers, R. A. Kik, M. M. E. Snel, R. A. Demel, J. A. Killian, J. van der Eerden, and B. de Kruijff. 2002. Domain formation in phosphatidylcholine bilayers containing transmembrane peptides: specific effects of flanking residues. *Biochemistry*. 41:2814–2824.
44. Mecke, A., S. Uppuluri, T. M. Sassanella, D. K. Lee, A. Ramamoorthy, J. R. Baker, B. G. Orr, and M. M. B. Holl. 2004. Direct observation of lipid bilayer disruption by poly(amidoamine) dendrimers. *Chem. Phys. Lipids*. 132:3–14.
45. Lam, K. L. H., Y. Ishitsuka, Y. S. Cheng, K. Chien, A. J. Waring, R. I. Lehrer, and K. Y. C. Lee. 2006. Mechanism of supported membrane disruption by antimicrobial peptide protegrin-1. *J. Phys. Chem.* 110: 21282–21286.
46. Jass, J., T. Tjarnhage, and G. Puu. 2000. From liposomes to supported, planar bilayer structures on hydrophilic and hydrophobic surfaces: an atomic force microscopy study. *Biophys. J.* 79:3153–3163.
47. Tokumasu, F., A. J. Jin, and J. A. Dvorak. 2002. Lipid membrane phase behaviour elucidated in real time by controlled environment atomic force microscopy. *J. Electron. Microsc. (Tokyo)*. 51:1–9.
48. Mechler, A., G. Nawaratna, M.-I. Aguilar, and L. L. Martin. 2006. A study of protein electrochemistry on a supported membrane electrode. *Int. J. Pept. Res. Ther.* 12:217–224.
49. Sauerbrey, G. 1959. Verwendung von Schwingquarzen zur Wägung dünner Schichten und zur Mikrowägung. *Z. Phys.* 155:206–222.